

# Phase Frustration-Induced Spatial Lattice Symmetry

Yichen Lu

July 19, 2025

## Contents

<b>1</b>	<b>The Model</b>	<b>1</b>
<b>2</b>	<b>Phase Frustration-Induced Crystallization</b>	<b>2</b>
2.1	Key properties . . . . .	2
2.1.1	Snapshots and phase diagram . . . . .	3
2.1.2	Respiration-like motion of unit cells . . . . .	9
2.1.3	Initial conditions determined cells composition . . . . .	11
<b>3</b>	<b>Critical condition for phase transition and mechanism</b>	<b>12</b>
3.1	Linear stability analysis with amplitude ansatz . . . . .	12
3.2	Abstract phase oscillator model . . . . .	13

## 1 The Model

Particles have a spatial position  $\mathbf{r}_i = (x_i, y_i)$  and an internal phase  $\theta_i$  which evolve according to equations:

$$\dot{\mathbf{r}}_i = v\mathbf{p}(\theta_i) , \quad (1a)$$

$$\dot{\theta}_i = \omega_i + \frac{K}{|A_i|} \sum_{j \in A_i} [\sin(\theta_j - \theta_i + \alpha) - \sin \alpha] , \quad (1b)$$

for  $i = 1, 2, \dots, N$ . Here in Eq. (1a),  $\mathbf{p}(\theta) = (\cos \theta, \sin \theta)$ , which means each particle rotates with a constant speed  $v$  in the direction of its instantaneous phase  $\theta_i(t)$ . The particles are treated as point-like with no direct spatial interactions, consistent with classical models of chiral self-propelled particles [1–3, 7, 8]. As per Eq. (1b), the mean runs over neighbors within a coupling radius  $d_0$  around particle  $i$ :

$$A_i(t) = \{j \mid |\mathbf{r}_i(t) - \mathbf{r}_j(t)| \leq d_0\} , \quad (2)$$

$K (\geq 0)$  is the coupling strength, and  $\{\omega_i\}$  are the natural frequencies distributed according to a given frequency distribution  $g(\omega)$ . This means that a particle will rotate with the angular velocity  $|\omega_i|$  in the absence of mutual coupling ( $K = 0$ ), and the sign of  $\omega_i$  represents the direction of rotation, namely, the tribute of the chirality of the  $i$ -th particle. A positive (negative) chirality ( $\omega$ ) describes the counterclockwise (clockwise) rotations of the particle in space.

Additionally,  $\alpha$  is the phase frustration between two neighboring particles. When  $\alpha_0 = 0$ , the dynamics reduces to the normal chiral model [4]. The counter term  $-\sin \alpha$  is introduced to ensure that frustration only interferes with the phase coupling without changing the sign of effective frequency.

The order parameter  $\sigma_\rho(t)$  is defined as the standard deviation of the density, which quantifies the degree of spatial ordering in the system.

$$\sigma_\rho(t) = \sqrt{\frac{1}{L^2} \int [\rho(\mathbf{r}, t) - \langle \rho(\mathbf{r}, t) \rangle]^2 d\mathbf{r}} , \quad (3)$$

where  $\rho(\mathbf{r}, t) = \int_0^{2\pi} f(\mathbf{r}, \theta, t) d\theta$  is the density of particles at position  $\mathbf{r}$  and time  $t$ , and  $\langle \rho(\mathbf{r}, t) \rangle = \frac{1}{L^2} \int \rho(\mathbf{r}, t) d\mathbf{r}$  is the average density over the system.

## 2 Phase Frustration-Induced Crystallization

### 2.1 Key properties

1. [Done] What does the lattice structure look like? What is the unit cell structure, and what is the spatial arrangement of the unit cells? Besides triangular, what other spatial structures exist? In which regions of frustration does it appear? (And what are the corresponding coupling conditions and natural frequency distributions?)

Lattice structure emerges when  $\alpha \in (\pi/2, \pi]$ . For  $\pi/2 < \alpha \ll \pi$ , the lattice structure exhibits a triangular arrangement (Sometimes it is a tetragonal lattice, but in most cases it is stable in a triangular lattice), where in each cell, particles are arranged in a vortex pattern independent of natural frequency (mainly determined by initial conditions). This arrangement leads to a stable and ordered configuration, where the cells maintain a fixed distance from each other and the particles rotate in a coordinated manner in the form of cycloids, which leads to respiration-like motion of the cells. While for  $\alpha = \pi$  (anti-alignment coupling), the system transforms into a double-lane structure with particles in each lane propelling in opposite directions.

2. [Done] What is each cell composed of?

Each cell is composed of particles with the neighboring particles at initial conditions, whose criterion is discussed in Sec. 2.1.3.

3. [Done] What is the internal dynamics within a cell?

Within a cell, particles are all-to-all coupled, and they rotate in a Kuramoto-like manner.

4. [Done] What determines the length (periodicity)? (Interaction distance?)

The lattice constant (distance) is determined by the coupling strength  $K$ , the radius  $d_0$ , and the frustration  $\alpha$ . For  $\alpha \gtrsim 0.5\pi$  The theoretical lattice constant is given by Eq. (5).

### 2.1.1 Snapshots and phase diagram

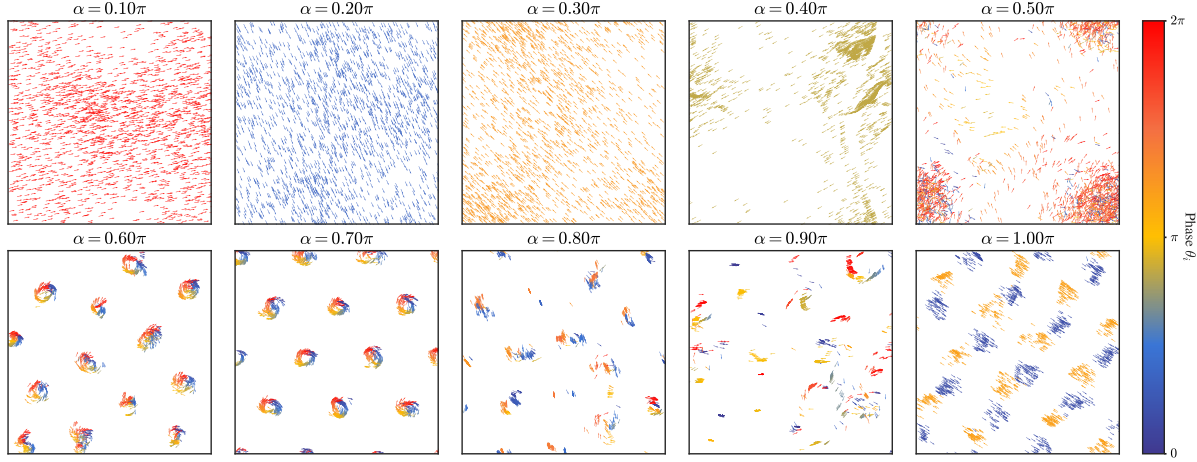


Figure 1: Snapshot of the achiral system ( $\omega_{\min} = 0$ ,  $\Delta\omega = 0$ ) at  $t = 200$  with  $N = 2000$ ,  $K = 16.83$ , and  $d_0 = 1.55$ .

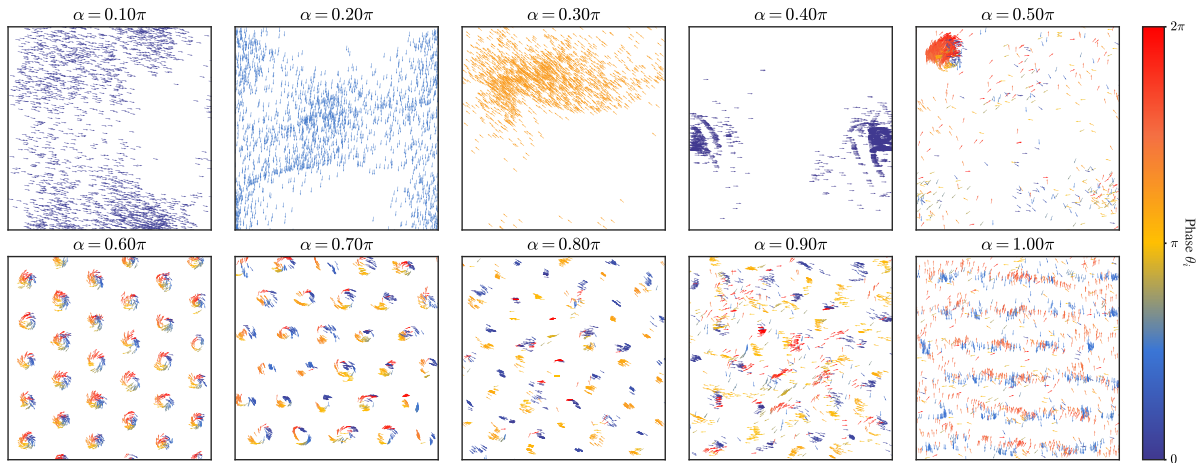


Figure 2: Snapshot of the achiral system ( $\omega_{\min} = 0$ ,  $\Delta\omega = 0$ ) at  $t = 200$  with  $N = 2000$ ,  $K = 20$ , and  $d_0 = 1$ .

The phase diagram of the system is constructed by varying the key parameters, including the coupling strength  $K$ , the radius  $d_0$ . The resulting patterns are classified into ordered and lattice states.

Single chirality particles can also form a triangular lattice structure:

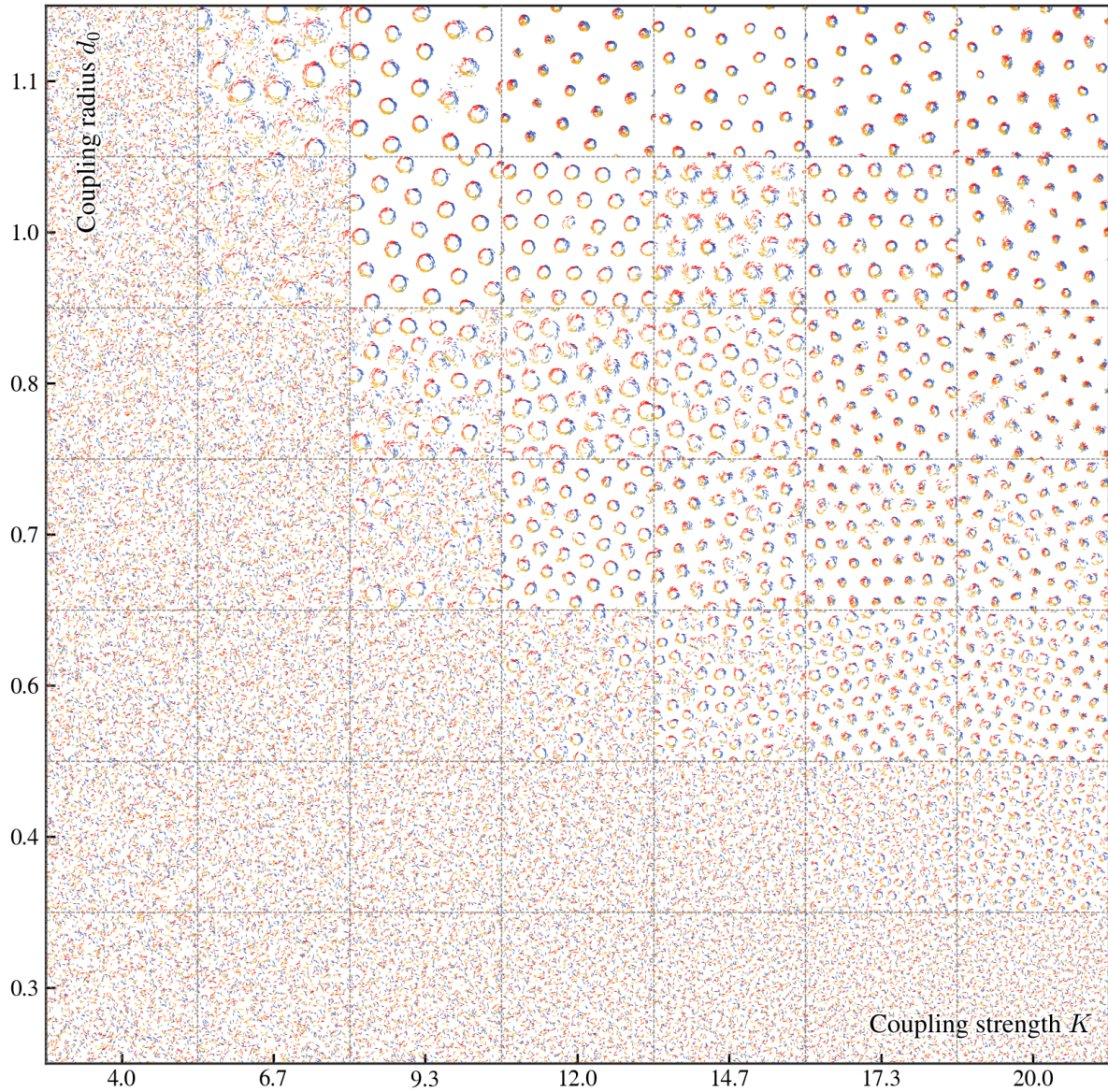


Figure 3: Snapshots of asymmetric chiral system ( $\omega_i \sim [0, 2]$ ) at different coupling strengths  $K$  and radius  $d_0$  for  $\alpha = 0.6\pi$ .

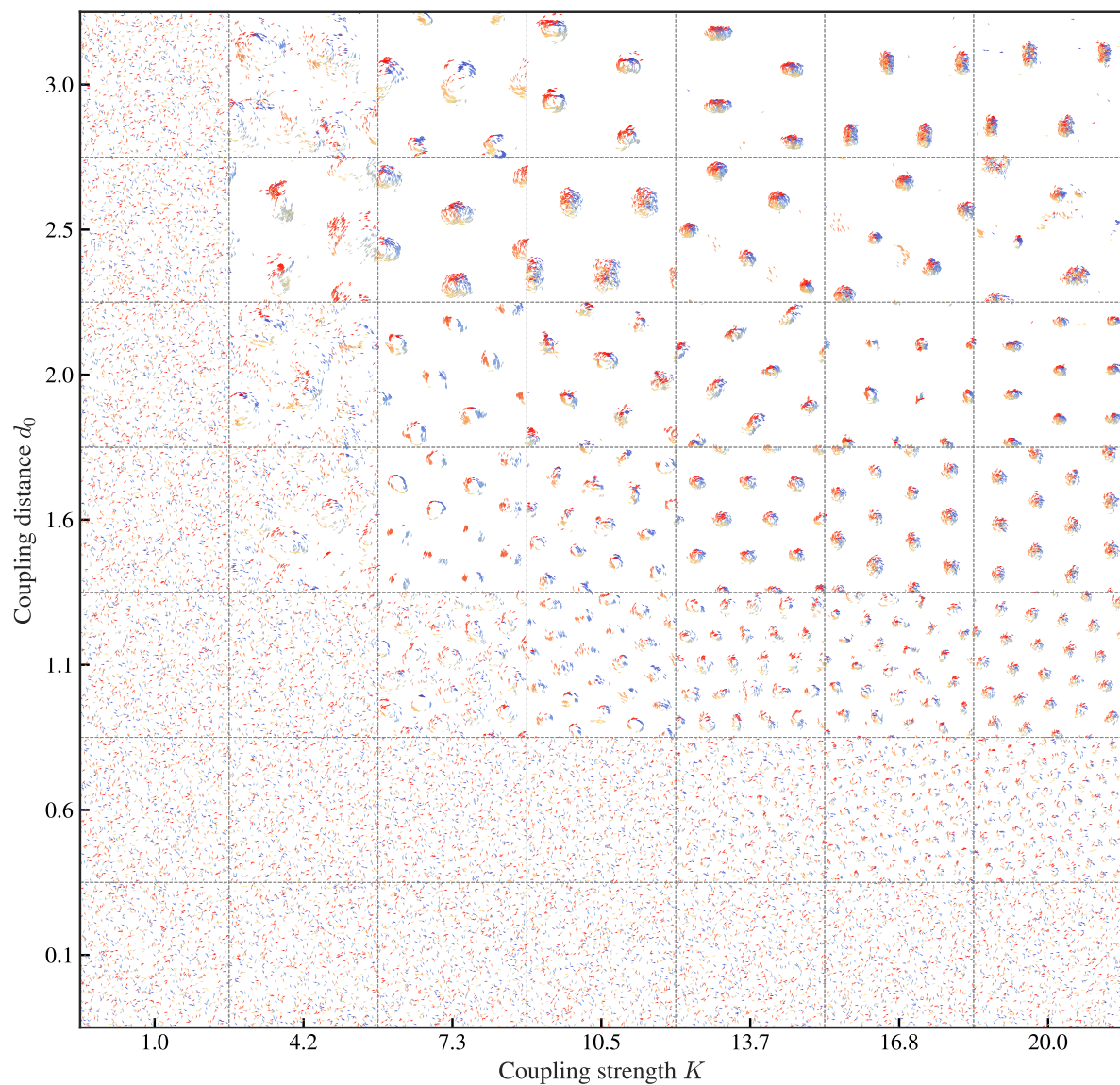


Figure 4: Snapshots of achiral system ( $\omega_{\min} = 0$  and  $\Delta\omega = 0$ ) at different coupling strengths  $K$  and radius  $d_0$  for  $\alpha = 0.6\pi$ .

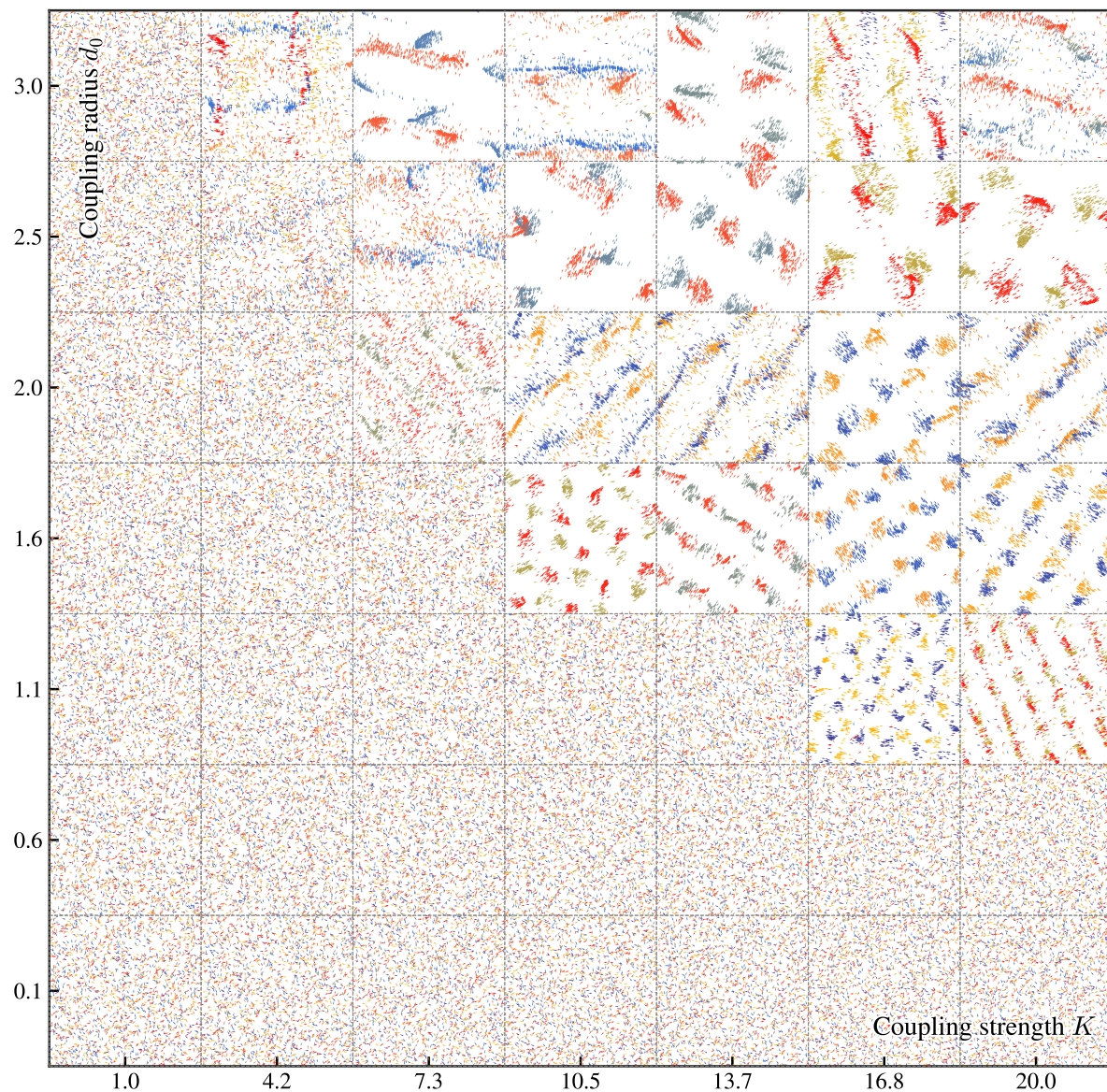


Figure 5: Snapshots of achiral system ( $\omega_{\min} = 0$  and  $\Delta\omega = 0$ ) at different coupling strengths  $K$  and radius  $d_0$  for  $\alpha = \pi$ .

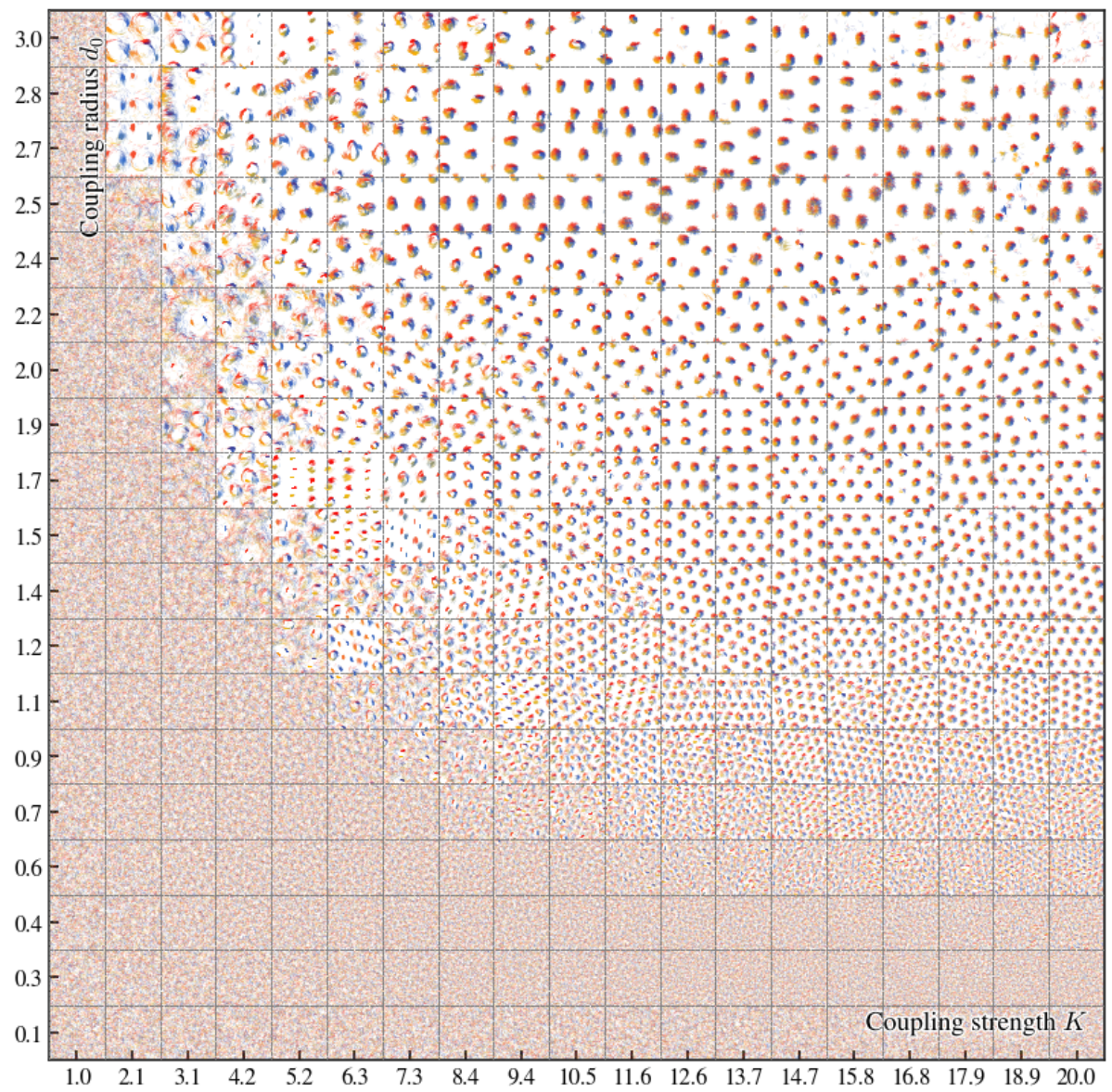


Figure 6: Snapshots of achiral system ( $\omega_{\min} = 0$  and  $\Delta\omega = 0$ ) at different coupling strengths  $K$  and radius  $d_0$  for  $\alpha = 0.6\pi$  with higher granularity.

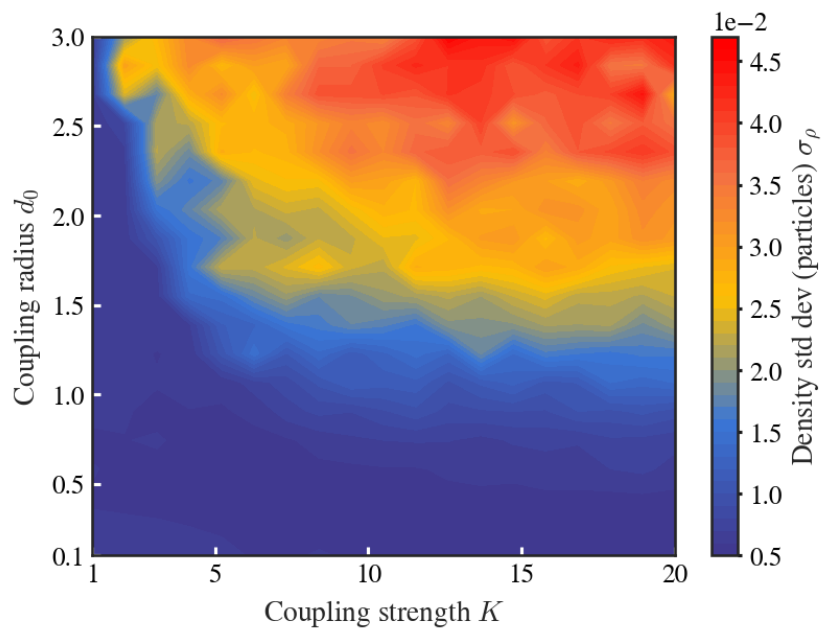


Figure 7: The order parameter  $\sigma_\rho(t)$  as a function of coupling strength  $K$  and radius  $d_0$  (Corresponding to Fig. 6). The color indicates the value of the order parameter.

### 2.1.2 Respiration-like motion of unit cells

For  $\alpha = 0.6\pi$ , the system exhibits the respiration-like motion of the cells. Since the phases of particles in each cell are uniformly distributed in  $[0, 2\pi]$  and the distance between cells is large enough to be considered decoupled, the effective frequency of each particle can be approximated by

$$\dot{\theta}_i = -K \sin \alpha + \frac{K}{|A_i|} \int_0^{2\pi} d\theta' \sin(\theta' - \theta_i + \alpha) = -K \sin \alpha , \quad (4)$$

and the lattice constant  $a$  can be approximated as

$$a = d_0 + 2 \frac{v}{K |\sin \alpha|} . \quad (5)$$

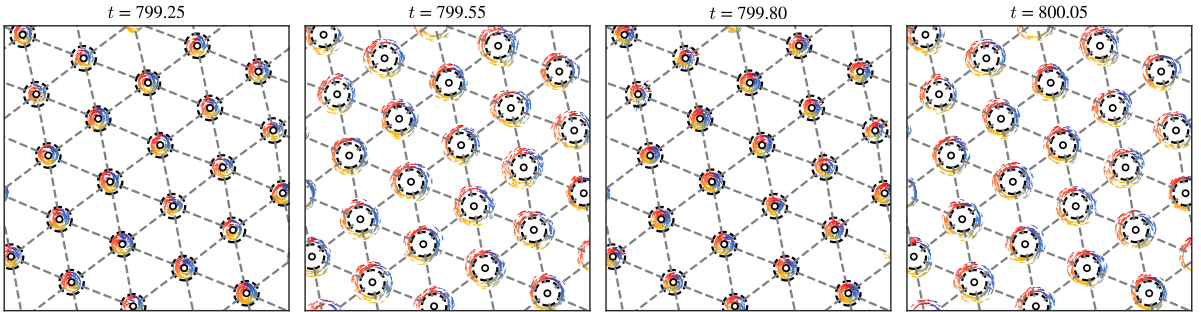


Figure 8: respiration-like motion of the cells at  $t = 200$  with  $\omega_{\min} = 0$ ,  $\Delta\omega = 0$ ,  $N = 2000$ ,  $K = 10.5$ ,  $d_0 = 1.07$ , and  $\alpha = 0.6\pi$ . Black hollow dots represent the center of mass of each cell, black dash circles represent the theoretical unit cell radius  $v/\dot{\theta}_i$ , and the gray dash lines represent the theoretical distance between unit cells  $d_0$ .

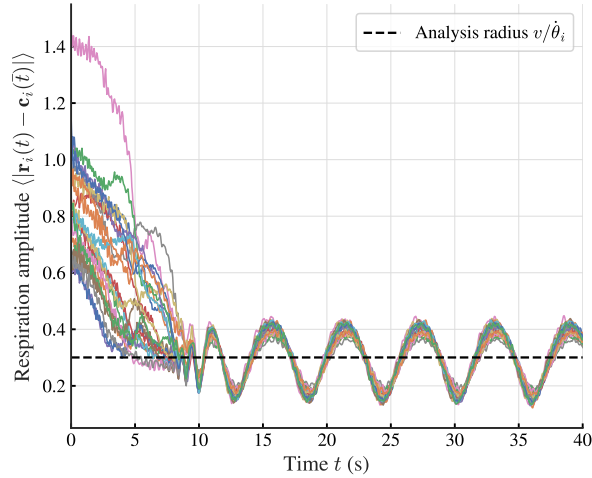


Figure 9: respiration amplitude of the system with  $\omega_{\min} = 0$ ,  $\Delta\omega = 0$ ,  $N = 2000$ ,  $K = 10.5$ ,  $d_0 = 1.07$ , and  $\alpha = 0.6\pi$ . Different colors represent different cells, and the amplitude is defined as the distance between particles and the center of mass of the cell at final state ( $\bar{t} = 40$ ).

As shown in Fig. 8 and Fig. 9, the respiration amplitude of the cells is defined as  $\langle |r_i(t) - c_i(\bar{t})| \rangle$ , where  $c_i(\bar{t})$  is the center of mass of the cell of  $i$ -th particle at final state ( $\bar{t} = 40$ ), and  $\langle \cdot \rangle$  denotes the average over all particles in the cell. It is worth noting that the amplitude is fluctuating around the theoretical cell radius  $v/\dot{\theta}_i$  and the respiration frequency of the cells exhibit synchronization.

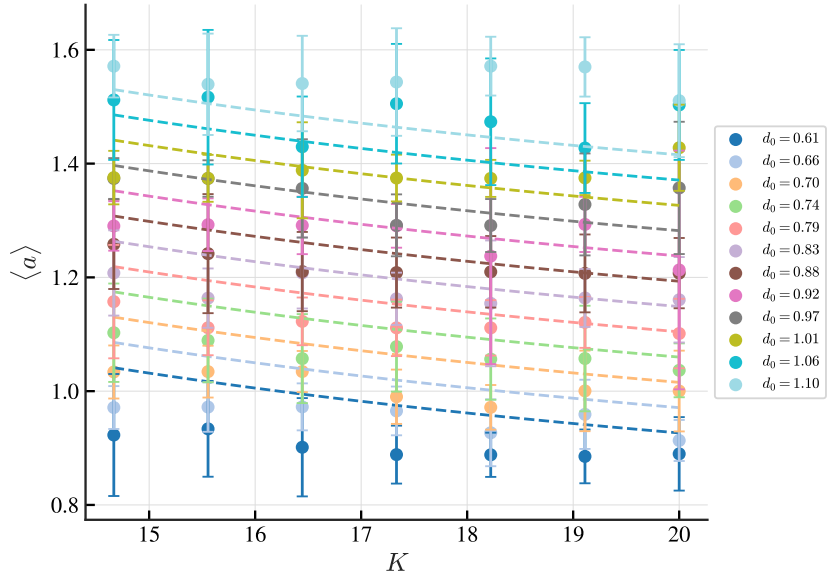


Figure 10: Lattice constant  $a$  as a function of coupling strength  $K$  and radius  $d_0$  for  $\alpha = 0.6\pi$ . The dash line represents the theoretical lattice constant  $a$  in Eq. (5).

### 2.1.3 Initial conditions determined cells composition

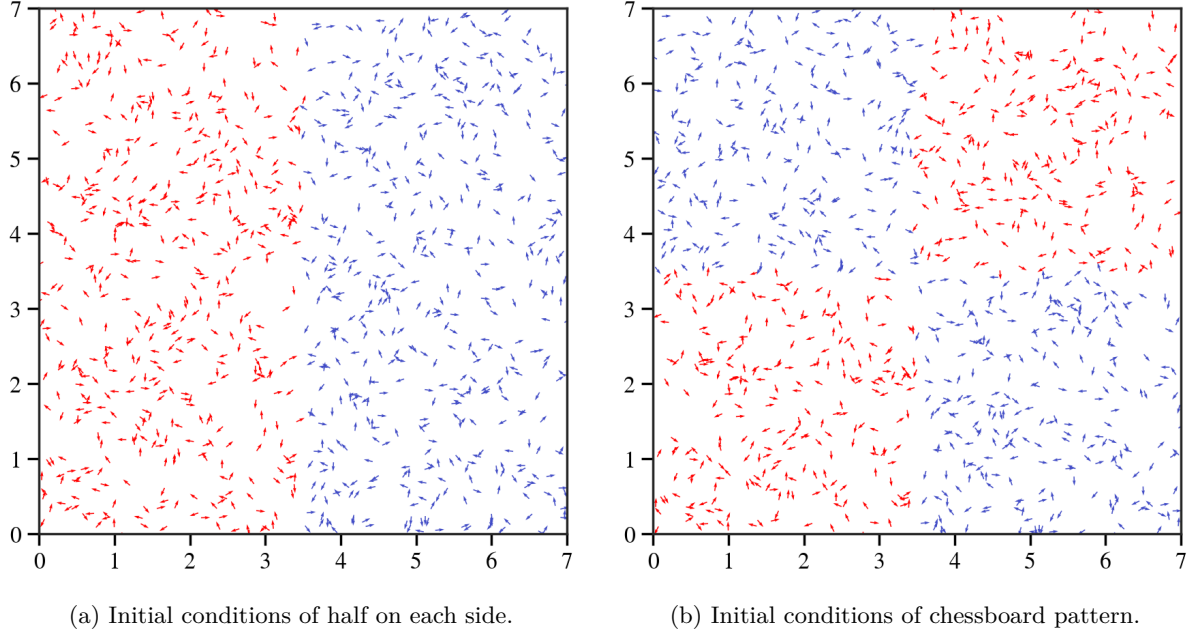


Figure 11: Two artificial non-uniform initial conditions in space. Red and blue particles represent particles with positive and negative chirality, respectively.

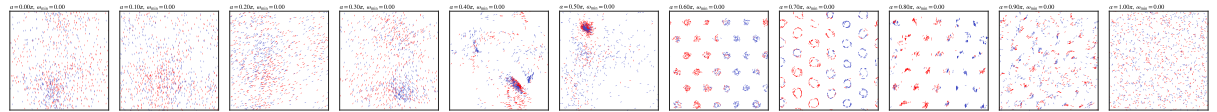


Figure 12: Snapshot of the system at  $t = 80$  with  $N = 1000$ ,  $K = 20$ ,  $\omega_{\min} = 0$ ,  $\Delta\omega = 1$  and initial conditions of half on each side.

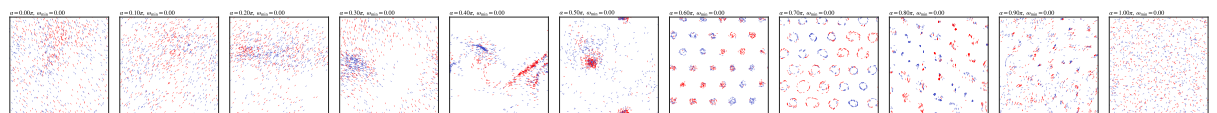


Figure 13: Snapshot of the system at  $t = 80$  with  $N = 1000$ ,  $K = 20$ ,  $\omega_{\min} = 0$ ,  $\Delta\omega = 1$  and initial conditions of chessboard pattern.

### 3 Critical condition for phase transition and mechanism

#### 3.1 Linear stability analysis with amplitude ansatz

##### Continuum Density Equation

$$\frac{\partial \rho}{\partial t} = -v \mathbf{p}(\theta) \cdot \nabla \rho - \frac{\partial}{\partial \theta} \{ \mathcal{T}[\rho] \rho \} \quad (6)$$

$$\mathcal{T}[\rho] = \frac{K}{A} \int \rho(\mathbf{r}', \theta', t) \Theta(\|\mathbf{r}' - \mathbf{r}\| - d_0) [\sin(\theta' - \theta + \alpha) - \sin \alpha] d^2 \mathbf{r}' d\theta' \quad (7)$$

$$A = \int \rho(\mathbf{r}', \theta', t) \Theta(\|\mathbf{r}' - \mathbf{r}\| - d_0) d^2 \mathbf{r}' d\theta' \quad (8)$$

##### Mean-Field Limit (Global Coupling)

$$p(\theta, t) = \int \rho(\mathbf{r}, \theta, t) d^2 \mathbf{r} \quad (9)$$

$$\frac{\partial p}{\partial t} = -\frac{\partial}{\partial \theta} \{ \mathcal{T}[\rho] p \} \quad (10)$$

$$\mathcal{T}[\rho] = K \int p(\theta', t) [\sin(\theta' - \theta + \alpha) - \sin \alpha] d\theta' \quad (11)$$

##### Linear Stability Analysis

$$p(\theta, t) = \frac{1}{2\pi} + \varepsilon e^{\lambda t} \Phi(\theta) \quad (12)$$

$$\lambda \Phi(\theta) = -\frac{\partial}{\partial \theta} \left\{ \frac{K}{2\pi} \int \Phi(\theta') [\sin(\theta' - \theta + \alpha) - \sin \alpha] d\theta' \right\} \quad (13)$$

##### Fourier Decomposition

$$\Phi(\theta) = \sum_{m=-\infty}^{\infty} c_m e^{im\theta} \quad (14)$$

$$\lambda_m = \frac{K}{2} (\delta_{m,-1} e^{i\alpha} + \delta_{m,1} e^{-i\alpha}) \quad (15)$$

##### Finite-Range Interactions

$$\rho(\mathbf{r}, \theta, t) = \frac{1}{2\pi L^2} + \varepsilon e^{\lambda(k)t+i\mathbf{k}\cdot\mathbf{r}} \Phi(\theta) \quad (16)$$

$$\mathcal{L} = \mathcal{L}_0 - ivk\mathcal{L}_1 \quad (17)$$

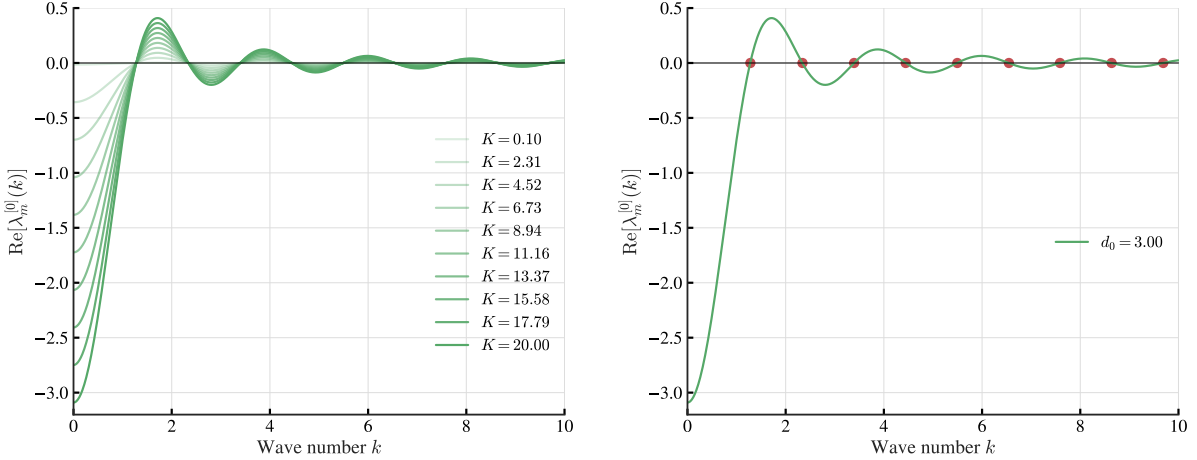
$$\mathcal{L}_0 \Phi = -\frac{K\Theta_k}{2\pi L^2 A} \frac{\partial}{\partial \theta} \left\{ \int \Phi(\theta') [\sin(\theta' - \theta + \alpha) - \sin \alpha] d\theta' \right\} \quad (18)$$

$$\mathcal{L}_1 \Phi = (\mathbf{p}(\theta) \cdot \hat{\mathbf{k}}) \Phi \quad (19)$$

$$\Theta_k = \begin{cases} \frac{2\pi d_0}{k} J_1(kd_0), & k \neq 0 \\ \pi d_0^2, & k = 0 \end{cases} \quad (20)$$

##### Eigenvalues

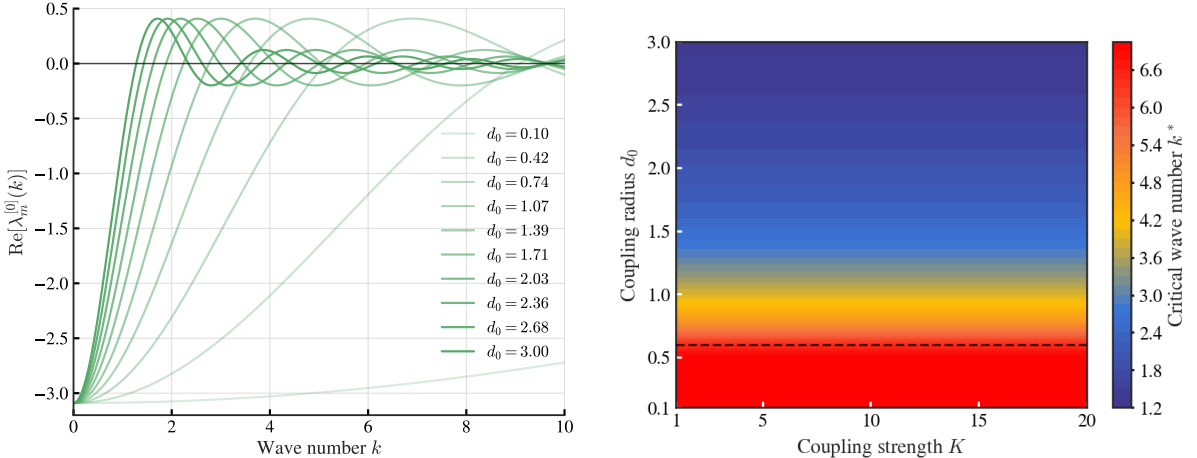
$$\lambda_m^{(0)}(k) = \frac{K\Theta_k}{2\Theta_0} (\delta_{m,-1} e^{i\alpha} + \delta_{m,1} e^{-i\alpha}) \quad (21)$$



(a)  $\text{Re}[\lambda_m^{[0]}(k)]$ . Different  $K$  have the same zero point.

(b) The zero point of  $\text{Re}[\lambda_m^{[0]}(k)]$  as a function of wave number  $k$ . The zero point solutions exhibit periodicity.

Figure 14: Simulation results for the linear stability analysis with  $K = 20$  and  $\alpha = 0.6\pi$ .



(a)  $\text{Re}[\lambda_m^{[0]}(k)]$ . The smaller  $d_0$ , the slower the instability speed, which corresponds to the simulation.

(b) Phase diagram of critical wave number  $k^*$  (first zero point of  $\text{Re}[\lambda_m^{[0]}(k)]$ ) as a function of  $(K, d_0)$ ,

Figure 15: Simulation results for the linear stability analysis with  $K = 20$  and  $\alpha = 0.6\pi$ .

### 3.2 Abstract phase oscillator model

Let us consider a decoupled phase-oscillator system

$$\dot{\theta}_i = \omega_i - K \sin \alpha + \frac{K}{N} \sum_{j=1}^N \sin(\theta_j - \theta_i + \alpha). \quad (22)$$

To quantify the phase coherence of the system, it is convenient to define the generalized complex-valued order parameters, i.e.,

$$Z(t) = R(t) e^{i\psi(t)} = \frac{1}{N} \sum_{j=1}^N e^{i\theta_j(t)}, \quad (23)$$

where  $n = 1, 2, \dots, N$ , and  $r(t)$ ,  $\psi(t)$  are the amplitudes and arguments of the order parameter. Our starting point is to analyze the critical point for the coherence of the order parameter. In the thermo-

dynamic limit  $N \rightarrow \infty$ , the state of the system in Eq. (22) can be characterized by the single-oscillator distribution  $\rho(\theta, \omega, t)$ , which satisfies the continuity equation

$$\frac{\partial \rho}{\partial t} + \frac{\partial(\rho v)}{\partial \theta} = 0, \quad (24)$$

where  $\rho(\theta, \omega, t)$  accounts for the fraction of oscillators with phase  $\theta$  lying in the interval  $(\theta, \theta + d\theta)$  at fixed frequency  $\omega$  and time  $t$ , it satisfies the normalization condition

$$\int_0^{2\pi} \rho(\theta, \omega, t) d\theta = 1. \quad (25)$$

Here,  $v(\theta, \omega, t)$  is the velocity field, given by

$$v(\theta, \omega, t) = K \int_{-\infty}^{+\infty} \int_0^{2\pi} \sin(\theta' - \theta + \alpha) \rho d\theta' d\omega' + \omega - K \sin \alpha. \quad (26)$$

Correspondingly, the order parameter defined in Eq. (23) in the thermodynamic limit reads

$$Z(t) = \int_{-\infty}^{+\infty} g(\omega) d\omega \int_0^{2\pi} e^{i\theta} \rho(\theta, \omega, t) d\theta, \quad (27)$$

then  $v(\theta, \omega, t)$  simplifies to

$$v(\theta, \omega, t) = \omega - K \sin \alpha + \text{Im}[H(t) e^{-i\theta}], \quad (28)$$

with the mean-field being

$$H(t) = K Z(t) e^{i\alpha}. \quad (29)$$

Since the distribution  $\rho(\theta, \omega, t)$  is  $2\pi$ -periodic in  $\theta$ , we can expand it in Fourier series as

$$\rho(\theta, \omega, t) = \frac{1}{2\pi} \sum_{n=-\infty}^{+\infty} a_n(\omega, t) e^{in\theta}, \quad (30)$$

where  $a_n(\omega, t)$  is the  $n$ -th Fourier coefficient. In particular, we have  $a_0(\omega, t) \equiv 1$  owing to the normalization condition in Eq. (25) and  $a_{-n}(\omega, t) = a_n^*(\omega, t)$ , where  $*$  denotes the complex conjugate.

According to the Ott-Antonsen ansatz [5, 6], it states that the  $n$ -th Fourier coefficient  $a_n(\omega, t)$  can be expressed in terms of the first-order coefficient, i.e.,  $a_n(\omega, t) = a^n(\omega, t)$ . In this regard, the evolution of  $\rho(\theta, \omega, t)$  degenerates to an invariant manifold, which is

$$\dot{a}(t) = i(K \sin \alpha - \omega) a(t) + \frac{1}{2} [H^*(t) - H(t) a^2(t)]. \quad (31)$$

Consequently, Eq. (31) is closed by the definition of the order parameter in Eq. (27), where

$$\begin{aligned} Z(t) &= \int_{-\infty}^{+\infty} g(\omega) a_{-1}(\omega, t) d\omega, \\ &= \int_{-\infty}^{+\infty} g(\omega) a^*(\omega, t) d\omega. \end{aligned} \quad (32)$$

We stress that Eq. (31) is still infinite dimensional because of the distributed natural frequencies. Thus, we may make a specific choice for the frequency distribution to get around this difficulty, e.g. a Lorentzian distribution  $g(\omega) = \Delta/[\pi(\omega - \mu)^2 + \Delta^2]$  with  $\Delta$  being the width of the distribution and  $\mu$  being the mean frequency. In this setting, the order parameters defined in Eq. (32) can be calculated by using Cauchy's residue theorem with analytical continuation of  $a(\omega, t)$  into the lower half complex plane, which leads to

$$Z(t) = a^*(\mu - i\Delta, t). \quad (33)$$

As a result, the low-dimensional evolution of the order parameter can be obtained by replacing  $\omega$  with  $\mu - i\Delta$  and by taking into account the complex conjugate, which reads

$$\dot{Z} = -\Delta Z + iZ(\mu - K \sin \alpha) + \frac{1}{2} [KZe^{i\alpha} - KZ^*Z^2e^{-i\alpha}] . \quad (34)$$

Rewrite above equation using polar coordinates  $Z(t) = R(t)e^{i\psi(t)}$ , we have

$$\dot{R} = \frac{R}{2} (K - 2\Delta - KR^2) \cos \alpha , \quad (35a)$$

$$\dot{\psi} = \mu + \frac{K}{2} (R^2 - 1) \sin \alpha . \quad (35b)$$

Obviously, the amplitude  $R(t)$  is decoupled from the mean phase  $\psi(t)$  and Eq. (35a) have a critical coupling strength  $K_c = 2\Delta$  and a pair of critical phase frustration  $|\alpha_c| = \pi/2$ . Let us first consider the simplest case of  $\Delta = 0, \mu = 0$ , which corresponds to the case of achiral particles. In this case, when  $|\alpha_c| > \pi/2$ , the system bifurcates to  $R = 0$ , which corresponds to the incoherent state in phase oscillators and lattice state in self-propelled particles, while for  $|\alpha_c| < \pi/2$ , the system has a unique stable fixed point at  $R = 1$ , which corresponds to the coherent state and swarming state, respectively.

For the incoherent state, the system is totally disordered with the phases distributed uniformly around the unit circle, i.e.,  $\rho(\theta, \omega, t) = g(\omega)/2\pi$ , which implies that the phase velocity of each oscillator/particle becomes

$$\dot{\theta}_i = \omega_i - K \sin \alpha . \quad (36)$$

Correspondingly, the rotational radii of  $i$ -th particle is

$$r_i = \frac{v}{\dot{\theta}_i} = \frac{v}{\omega_i - K \sin \alpha} . \quad (37)$$

## References

- [1] Michel Fruchart, Ryo Hanai, Peter B. Littlewood, and Vincenzo Vitelli. Non-reciprocal phase transitions. *Nature*, 592(7854):363–369, Apr 2021.
- [2] D. Levis, I. Pagonabarraga, and B. Liebchen. Activity induced synchronization: Mutual flocking and chiral self-sorting. *Phys. Rev. Res.*, 1:023026, Sep 2019.
- [3] Benno Liebchen and Demian Levis. Collective behavior of chiral active matter: Pattern formation and enhanced flocking. *Phys. Rev. Lett.*, 119:058002, Aug 2017.
- [4] Yichen Lu, Yixin Xu, Wanrou Cai, Zhuanghe Tian, Jie Xu, Simin Wang, Tong Zhu, Yali Liu, Mengchu Wang, Yilin Zhou, Chengxu Yan, Chenlu Li, and Zhigang Zheng. Self-organized circling, clustering and swarming in populations of chiral swarmalators. *Chaos, Solitons & Fractals*, 191:115794, 2025.
- [5] Edward Ott and Thomas M. Antonsen. Low dimensional behavior of large systems of globally coupled oscillators. *Chaos: An Interdisciplinary Journal of Nonlinear Science*, 18(3):037113, 09 2008.
- [6] Edward Ott and Thomas M. Antonsen. Long time evolution of phase oscillator systems. *Chaos: An Interdisciplinary Journal of Nonlinear Science*, 19(2):023117, 05 2009.
- [7] Bruno Ventejou, Hugues Chaté, Raul Montagne, and Xia-qing Shi. Susceptibility of orientationally ordered active matter to chirality disorder. *Phys. Rev. Lett.*, 127:238001, Nov 2021.
- [8] Yujia Wang, Bruno Ventéjou, Hugues Chaté, and Xia-qing Shi. Condensation and synchronization in aligning chiral active matter. *Phys. Rev. Lett.*, 133:258302, Dec 2024.